



Study on Representative Volume Elements Considering Inhomogeneity and Anisotropy of Rock Masses Characterised by Non-persistent Fractures

Wenliang Ma¹ · Huie Chen¹ · Wen Zhang¹ · Chun Tan^{2,3} · Zhenbang Nie¹ · Jia Wang¹ · Qi Sun¹

Received: 4 August 2020 / Accepted: 4 June 2021 / Published online: 1 July 2021
© The Author(s), under exclusive licence to Springer-Verlag GmbH Austria, part of Springer Nature 2021

Abstract

This study takes the rock masses in the dam foundation of a sluice gate of the Datengxia Hydropower Station in China as a case study to determine the geometrical and mechanical representative volume elements (RVEs) considering the special natures of rock masses (inhomogeneity and anisotropy). 3D fracture networks are generated on the basis of fracture data in the field and then used in this study for RVE determination. The representative parameters for RVE determination are selected and presented first. Through the comparison and analysis of the RVEs in different regions and directions, it is discovered that the inhomogeneity and anisotropy of the rock result in the spatial effect and directional effect in the RVE size, respectively. Therefore, the traditional method of RVE determination needs to be improved. Subsequently, on the basis of the sampling methods considering the special natures, the special natures of the geometrical and mechanical parameters are studied in detail and fully considered to improve the accuracy of the RVE results. Finally, the geometrical RVE size (10 m) and mechanical RVE size (18 m) are determined with the coefficient of variation. Moreover, the relationship between the geometrical and mechanical RVE sizes is also established.

Keywords Representative volume element · 3D fracture network · Geometrical · Mechanical · Inhomogeneity · Anisotropy

Abbreviations

r	Fracture disc diameter
L	The height of 3D space that accommodates the fractures
θ	The intersection angle between the fracture set and the outcrop surface
α	The average intersection angle between the fractures and the outcrop surface
p_n	The frequency of fractures in the equal-area Schmidt projection diagram
N_α	The number of fractures with an intersection angle of α in the outcrop surface

P_α	The corrected fracture frequency with an intersection angle of α in 3D space
L_{\min}	The minimum side length of the model
n_{ab}	The number of fractures with radii between a and b in the outcrop surface
n'_{ab}	The number of fractures with radii between a and b in 3D space
RES	The number of particles within the minimum side length of the model

1 Introduction

A large number of discontinuities may develop in rock masses. Such discontinuities may be large-scale structures, such as faults and bedding planes that extend to tens or hundreds of metres, or medium- to small-scale structures, such as joints and foliations that extend from a few centimetres to tens of metres (Esmaili et al. 2010). These discontinuities result in the inhomogeneity and anisotropy of rock masses and a prominent scale effect on rock mass properties (Wu and Kulatilake 2012; Yong et al. 2018). An essential way to quantify the scale effect is to use the

✉ Wen Zhang
zhang_wen@jlu.edu.cn

¹ College of Construction Engineering, Jilin University, Changchun 130026, Jilin, China

² China Water Northeastern Investigation, Design and Research Co., Ltd., Changchun 130026, Jilin, China

³ North China Power Engineering Co., Ltd., of the China Power Engineering Consulting Group, Changchun 130000, Jilin, China

representative volume element (RVE). When the size of a rock mass is equal to or larger than the RVE size, the fluctuation in the rock properties significantly decreases. In this case, the properties of the rock mass with the RVE size effectively represent those of the whole rock mass. Similarly, in the analysis of rock mass engineering problems through numerical simulation methods, the continuum model is only applicable when the divided units are equal to or larger than the RVE (Zhang et al. 2013a; Liu et al. 2018). Therefore, RVE determination plays a fundamental role in the analysis of rock mass problems.

The concept of RVE was first proposed in a study on the seepage of porous media by Bear (1972). Subsequent studies on RVE were carried out in various fields, and different determination methods were proposed. Pinto and Da (1993) determined the mechanical RVE size with in situ tests. However, such tests are extremely difficult and expensive. Numerical simulations were then widely used by scholars. Karatlike (1985) and Shalhoob and Poufy (2008) investigated mechanical RVEs with the finite element method. Min et al. (2004) and Wu and Kulatilake (2012) used field data to generate 3D fracture network models, and the RVE sizes based on the mechanical properties were studied with the distinct element method. Esmaili et al. (2010) studied the scale effect on the geometrical and mechanical properties of rock mass and determined geometrical and mechanical RVE sizes with the three-dimensional Particle Flow Code (PFC3D, Itasca Co. Ltd.). In addition, given the random distribution of fractures in rock masses, statistical tests were widely used to determine RVE. Li et al. (2017) applied the Mann–Whitney test to determine the RVE based on the fracture connectivity parameters. Liu et al. (2018) studied the inhomogeneity of volumetric fracture density (P_{32}) in rock masses and determined the RVE based on P_{32} with the likelihood ratio test and Wald–Wolfowitz runs test.

In the past few decades, many properties of rock masses have been investigated in RVE studies. These studies can be divided mainly into two categories in terms of the parameters (i.e. geometrical and mechanical parameters). Geometrical parameters include P_{32} , the fracture orientation, the rock quality designation, the fracture connectivity, the fracture persistence, etc. (Esmaili et al. 2010; Zhang et al. 2012, 2013a, 2013b; Li et al. 2017; Song et al. 2017). The RVEs based on the aforementioned parameters are usually referred to as geometrical RVEs, for which many statistical methods are used to obtain the parameters. Mechanical parameters include Young's modulus, the deformation modulus, Poisson's ratio, the uniaxial compressive strength, the damage coefficient, etc. (Castelli et al. 2003; Ivars et al. 2008; Esmaili et al. 2010; Wu and Kulatilake 2012; Ni et al. 2016). Due to the limitation of site conditions and the high costs of in situ and laboratory tests, numerical simulation

tests are usually used to obtain the parameters for mechanical RVE determination.

This study takes a large field outcrop downstream of a sluice under construction as a study area. The number of fractures and the information of the geometrical characteristics collected are sufficient to support the reasonable modelling of the 3D fracture network of field rock masses to study the RVE. The study results will contribute on the analysis of engineering problems of this station. The correlational study on geometrical and mechanical RVEs is necessary for the in-depth study of RVEs and the size effects on various parameters. Although previous studies have involved this kind of work (Esmaili et al. 2010), the selection of parameters in RVE determination is important to be discussed due to the great influence of the selected parameters on the RVE size. Moreover, rock masses characterised by non-persistent fractures are inhomogeneous and anisotropic (described as special natures in this article). Some researchers took inhomogeneity into account using non-parametric hypothesis tests in the studies of geometrical RVE (Li et al. 2017; Liu et al. 2018). At present, the study on the special natures is not systematic in RVE determination. It is necessary to analyse the effects of the special natures on the various RVE sizes and comprehensively consider them to accurately determine the RVE sizes. The deep exploration and accurate determination of RVE lay a foundation for the analysis of engineering problems.

The current study considers the rock masses downstream of the sluice gate at Datengxia Hydropower Station in a case study to establish a comprehensive analysis of these problems. In this study, 3D fracture networks are generated on the basis of the fractures collected from the field (Sect. 2). On the premise of the reasonable selection and presentation of the parameters (Sect. 3), the geometrical and mechanical RVEs are determined, in which the special natures of rock masses are considered, and the effects of the special natures on the RVEs are analysed (Sect. 4). Finally, the relationship between the geometrical and mechanical RVEs under confining pressure are studied (Sect. 5).

2 Generation of a 3D Fracture Network

2.1 Study Area

Rock masses at the Datengxia Hydropower Station are investigated in this study. The station is located in the Qian Jiang River, a branch of the Pearl River in Guiping City, Guangxi Province, China (Fig. 1). It is listed as a major project of the Minister of Water Resource. The main engineering tasks of the station are flood control, power generation and water resource allocation. The main dam is a concrete gravity dam with a length of 1343 m and a maximum height of 80 m. The

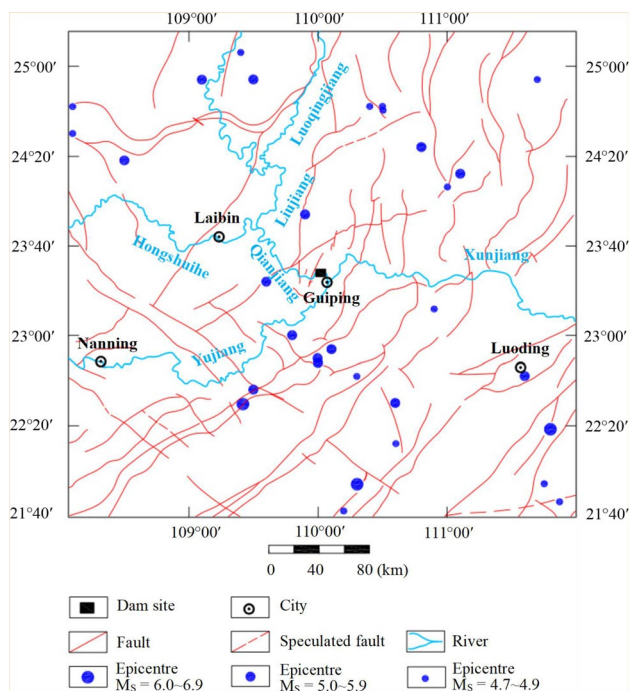


Fig. 1 Location map of the Datengxia Hydropower Station

following data are forecasted after the completion of engineering: normal water level of 61 m, total storage capacity of 3.43 billion m³, installed power station capacity of 1.6 million kWh and annual power output of 6.13 billion kWh.

No earthquake with a magnitude equal to or larger than 7.0 has been recorded in this area, but three earthquakes with magnitudes of 6.0–6.9 were recorded in recent decades (Fig. 1). The nearest distance between the dam site and the epicentre of an earthquake with a magnitude of 6.0–6.9 is approximately 120 km. In the reservoir area, the seismic activity is weak.

The lithologies of the reservoir area are characterised by sedimentary rocks from Cambrian to Quaternary systems, while Ordovician, Silurian and Jurassic systems are lacking. The exposed strata of the reservoir area are mainly the Lower Devonian system (D₁), with lithologies of limestone and mudstone (Fig. 2).

The sluice gate, in sections #23–33, is an important part of the main dam (Fig. 3). This gate is estimated to bear high hydrostatic pressures exerted by an upstream water level of 61 m and a downstream water level of 22.7 m (normal storage conditions). In addition, the rock masses downstream of the sluice gate are poor due to a large number of discontinuities, as shown in Fig. 3. Thus, the rock masses of the dam foundation of the sluice gate are more prone to damage than other parts. This part of the rock masses needs to be studied

Fig. 2 Geological map of the Datengxia Hydropower Station and photographs of the study area and fracture collection domain

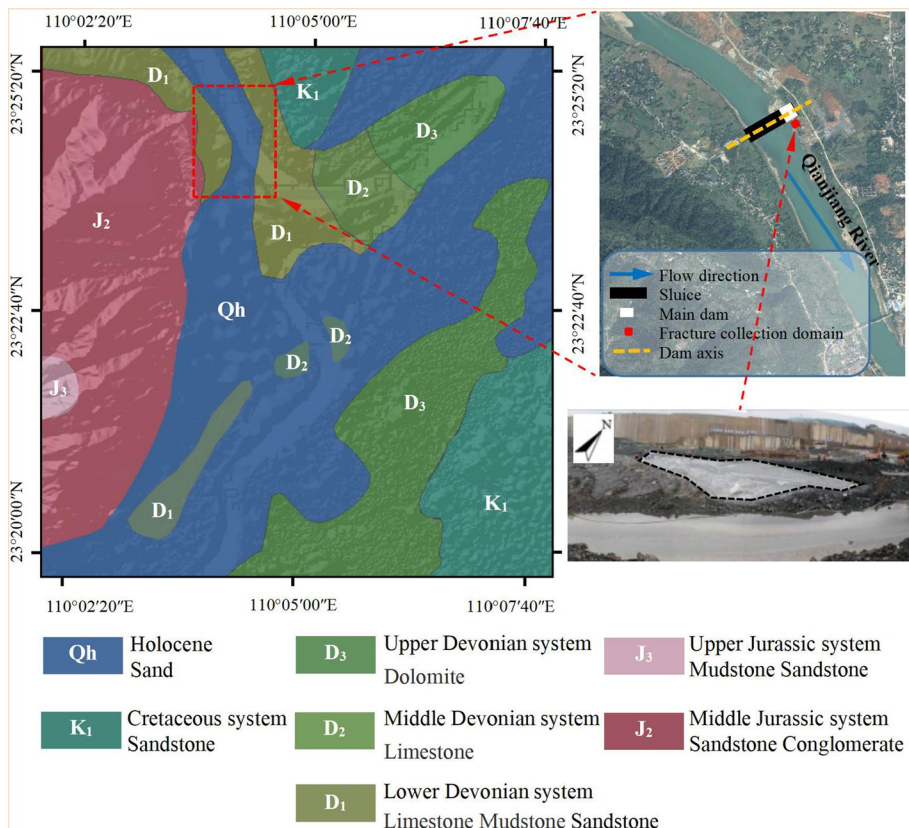
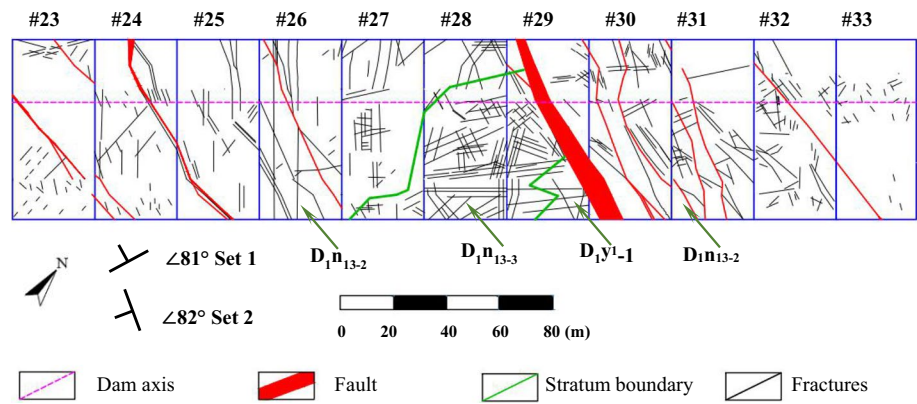


Fig. 3 Structural geological graph of the rock masses beneath the sluice gate



in depth, including the relevant size effects and RVEs based on different geometrical and mechanical considerations.

The main strata downstream of the sluice gate are mudstone and sandstone from the 13th layer of the Nagaolingian and limestone from the Lower Yujiangian. These two strata have similar bedding orientations of $N5^\circ-20^\circ E$, $SE\angle 10^\circ-15^\circ$. The structure, mineral composition and colour of the rock masses are almost unchanged. The partial fracture surfaces are slightly discoloured. The rock masses are weakly weathered.

Few faults are developed around the sluice gate, and the widths of the crushed zones are relatively small, except for that of the F216 fault. The faults intersect the dam axis at a large angle.

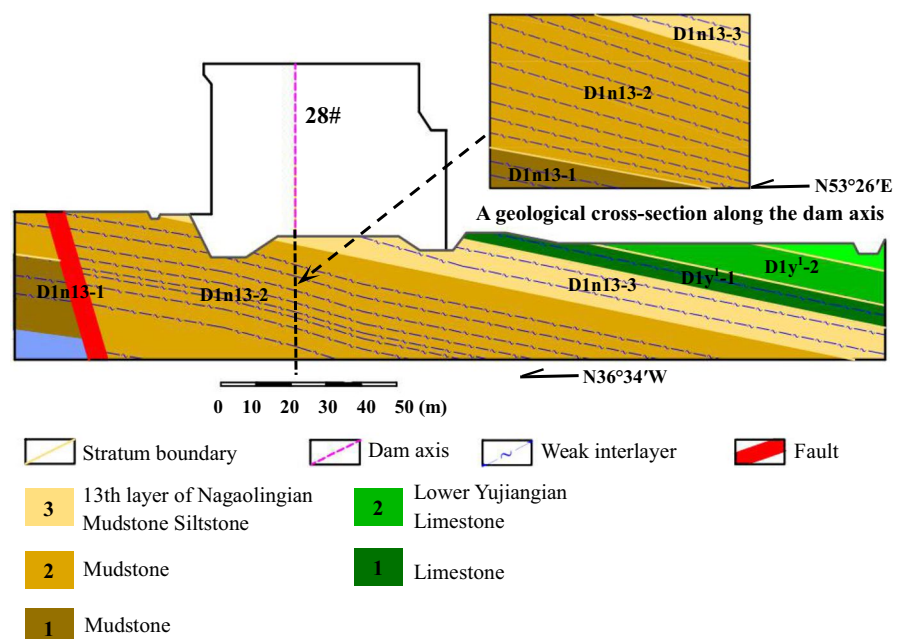
A large number of stochastic fractures are exposed beneath the slice gate (Fig. 3). Different from the configurations of the other sections, the features of fractures in section #28 are special. The size and density of the fractures are

large. Moreover, many of the fractures are nearly parallel to the dam axis. When the fractures intersect bedding planes and weak interlayers, failure surfaces are likely to develop (Fig. 4). Therefore, this study focuses on the rock masses downstream of section #28.

2.2 Acquisition of Fracture Data

A horizontal artificially excavated outcrop with an area of 807.3 m^2 at D_1y^1-2 downstream of section #28 is used for the collection of fractures, as shown in Fig. 2. Fractures with trace lengths longer than 0.5 m are collected using the sampling window method (Kulatilake and Wu 1984). The geometrical characteristics, including the location (start and end coordinates), orientation (dip direction and dip angle), aperture, surface roughness of the fracture wall and filling, are recorded. Data form a total of 390 fractures are collected from the field. The fracture traces are shown in Fig. 5.

Fig. 4 Geological structure profile around section #28



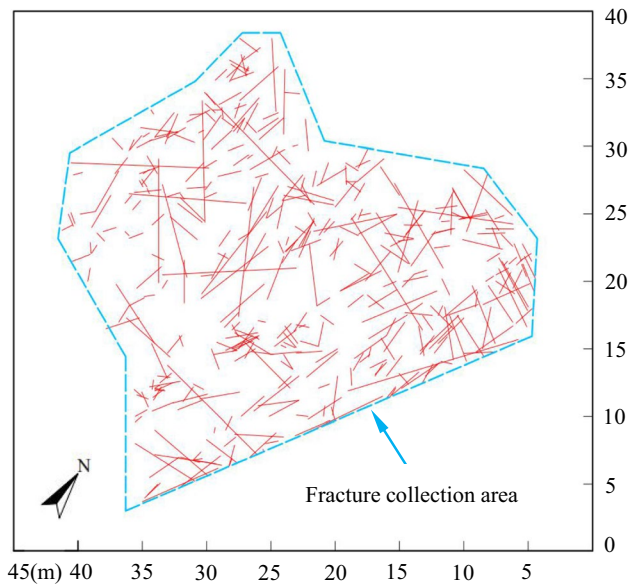


Fig. 5 Trace of the fractures collected from the outcrop surface

The trace lengths of the fractures are mostly shorter than 4 m, with an average value of 2 m and minimum and maximum lengths of 0.5 m and 13.7 m, respectively. Most of the fractures have steep dip angles greater than 60° . The apertures commonly range from 1 to 3 mm. The fracture walls mainly present a straight and smooth morphology, with fewer presenting a wavy morphology. The fillings are mainly rock debris and weathered muds. The persistence of these fractures is 46%. The grouping results are obtained using the method proposed by Shanley and Mahtab (1976), as shown in Fig. 6 and Table 1. The directions of the predominant fracture sets are shown in Figs. 3 and 6. Set 1 intersects the dam axis at a relatively small angle, and set 2 intersects the dam axis at a large angle.

2.3 3D Fracture Network Modelling

Influenced by tectogenesis, many stochastic fractures are developed inside the D_1y^{1-2} rock masses. However, only 2D trace information can be obtained by field investigation. Consequently, obtaining 3D fractures information through a modelling method is necessary to analyse the size effect and determine the RVE from a 3D perspective (Zhang et al. 2020b).

In consideration of the size of the sampling window (approximately $40\text{ m} \times 30\text{ m}$) and the thickness of stratum D_1y^{1-2} ($20 \sim 30\text{ m}$), a model with dimensions of $50\text{ m} \times 40\text{ m} \times 40\text{ m}$ is designed to accommodate the 3D fracture network. A 3D fracture network modelling method suitable for large fracture windows was proposed

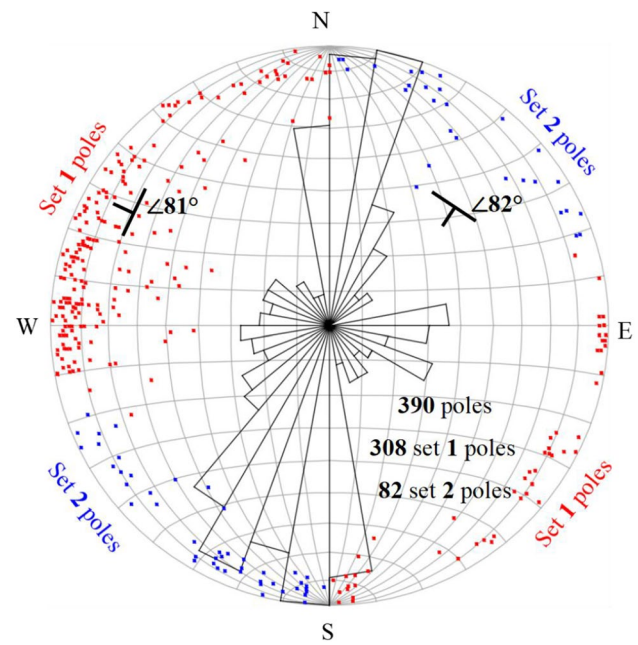


Fig. 6 Strike rose diagrams and the poles of the 390 fractures collected from the field

by Nie et al. (2019) with disc-shape discontinuities. 3D fracture network modelling is carried out on the basis of this fracture geometry. The steps are as follows:

(1) Determination of statistical homogeneity and preferential fracture sets.

The number of fractures is limited in the field. The division of the statistical homogeneity greatly decreases the accuracy of the fracture statistical results. The lithology and strength of the rock is uniform in the study area, suggesting that the characteristics of the fractures are similar in different locations. In addition, the inhomogeneity of the fractures can be statistically accepted to model the 3D fracture network. Therefore, the rock masses in the study area can be regarded as a statistically homogeneous zone (Zhang et al. 2013a, 2013b). The fractures are demarcated into two sets based on orientation (Table 1, Fig. 6). These two fracture sets are separately modelled to generate 3D fracture networks.

(2) Determination of fracture disc diameter $2r$.

The stochastic mathematical method is used to determine the probability density function (PDF) of r . The mean, variance and probability density distribution type of r are determined on the basis of the field trace length data using the trial method and chi-square test (Bryant and Satorra 2012). Subsequently, the PDF of r that intersects the outcrop surface is obtained. However, in actual cases, the PDF of r differs from that in 3D space. Thus, a correction is carried out using Eq. (1).

Table 1 Parameters of the two fracture sets collected from the field

Fracture set	Fracture number	Dip direction (°)		Dip angle (°)		Trace length (m)		Frequency	
		Mean	Std	Mean	Std	Mean	Std	P ₂₀ (m ⁻²)	P ₂₁ (m/m ²)
1	308	294	27.67	81	8.45	2.19	1.87	0.3815	0.8270
2	82	212	20.43	82	6.36	2.03	1.53	0.1016	0.2033

$$n'_{ab} = \frac{n_{ab}}{\int_a^b \frac{2r \sin \theta}{L} dr}, \tag{1}$$

where n_{ab} and n'_{ab} are the number of fractures with radii between a and b in the outcrop surface and in 3D space, L is the height of the 3D space that accommodates the fractures, and θ is the intersection angle between the fracture set and the outcrop surface.

(3) Determination of fracture orientation.

Although the orientations of the fractures in the outcrop surface are collected from those in 3D space, the frequencies of the fracture orientation in 3D space may differ from those collected from the outcrop surface (Terzaghi 1965). For example, the probability that fractures that intersect the outcrop surface at small angles are collected is smaller than that of fractures with large angles. Equation (2) is used accordingly to correct this deviation.

$$P_\alpha = \left(\frac{N_\alpha}{\sin \alpha} \right) / \left(\sum \frac{N_\alpha}{\sin \alpha} \right), \tag{2}$$

where α is the average intersection angle between the fractures and the outcrop surface, N_α is the number of fractures with an intersection angle of α in the outcrop surface, and P_α is the corrected fracture frequency with an intersection angle of α in 3D space.

(4) Determination of fracture density.

The density of the fractures is determined by the trial method. An arbitrary density is assumed to determine the fracture number n in 3D space. A 3D fracture network is generated on the basis of the aforementioned radii, orientations and n . Subsequently, this 3D fracture network is intersected by a plane with an orientation identical to that of the outcrop surface. The density is adjusted until the number of fractures intersecting the plane in 3D space is consistent with that in the outcrop surface, i.e. the trial method.

(5) Monte Carlo simulation.

The fracture centre points are assumed to follow a homogeneous (Poisson) model (Billaux et al. 1989); thus, n centre coordinates are stochastically generated. Then, n random fracture diameters and orientations are generated according to Steps 2 and 3. Finally, n diameters and orientations are stochastically combined to generate 3D fracture networks (Li et al. 2020).

(6) Verification of the 3D fracture networks.

The generated networks are intersected by a plane with an orientation identical to that of the outcrop surface. If the statistical characteristics of the fracture traces in the intersection plane are consistent with those in the outcrop surface, the networks are reasonable. The Fisher constant is used to represent the fracture orientation distribution. The fracture number and P_{21} (m/m²) are used to represent the fracture density. The average and standard deviation are selected as the statistical characteristics of trace length. The statistical parameters in the intersection plane and outcrop surface are calculated, and the results are shown in Table 2. The statistical parameters are nearly the same, indicating that the simulated networks are reasonable.

The parameters of the fracture sets for 3D fracture network modelling are determined and verified on the basis of the aforementioned steps. The details are shown in Table 3. The 3D fracture networks of the two fracture sets are separately generated, in which the fractures are numerically expressed by their coordinates, sizes and orientations. Figure 7 shows the 3D fracture networks using a discrete fracture network (DFN) in PFC3D, which are accommodated in domains with a size of 50 m × 40 m × 40 m.

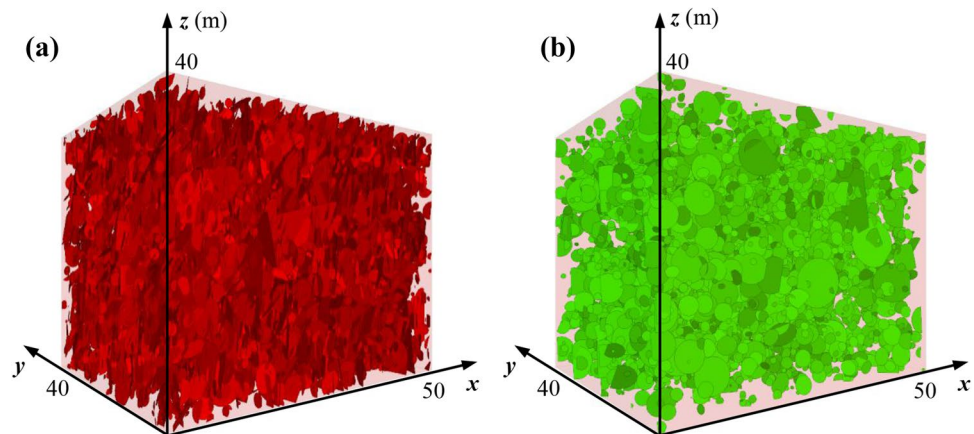
Table 2 Comparison of the statistical parameters between the intersection plane and outcrop surface

Fracture set		Fisher constant	Fracture number	P ₂₁ (m/m ²)	Trace length	
					Average	Standard deviation
1	Intersection plane	10.1883	304	0.8329	2.2099	1.7606
	Outcrop surface	9.8799	305	0.8270	2.1891	1.8697
2	Intersection plane	13.7779	82	0.1971	1.9583	1.4749
	Outcrop surface	14.8824	81	0.2033	2.0267	1.5338

Table 3 Parameters of the two fracture sets for 3D fracture network modelling

Fracture set	r in 3D space					Average orientation	Density (m^{-3})
	Distribution type	Mean	Variance	μ^a	σ^b		
1	Lognormal	0.97	0.45	-0.22	0.63	294°∠81°	0.2038
2	Lognormal	0.88	0.35	-0.31	0.61	212°∠82°	0.0588

^a the identical location parameter and ^b the scale parameter in a lognormal distribution

Fig. 7 3D fracture networks of the two fracture sets: (a) set 1 and (b) set 2

3 Key Conditions of RVE Determination

Several key conditions need to be exhibited prior to RVE determination. In the present study, we select the representative parameters to determinate the geometrical and mechanical RVEs. Then, we state the sampling principles to explain how the special natures can be taken into account. Finally, the RVEs can be easily determined by the quantitative method.

3.1 Parameter Selection

The RVE sizes of rock masses greatly depend on the parameters considered. The selection of parameters must be reasonable enough to ensure that the determined RVEs can accurately represent the geometrical and mechanical characteristics of the whole rock masses.

3.1.1 Geometrical Parameters

Density, size and orientation, the basic geometrical characteristics of fractures, can be used to characterise the fracture structures in rock masses. Therefore, the selected parameters for RVE determination need to reflect the aforementioned geometrical elements. In this way, the determined RVE can accurately represent the geometrical characteristics of the rock masses. Volumetric fracture density (P_{32}), which can simultaneously represent size and density, and patches in the

equal-area Schmidt projection diagram, which can represent orientation information, are selected as the parameters for geometrical RVE determination in the present study.

3.1.2 Mechanical Parameters

An accurate understanding of rock mass strength and deformability is fundamental to ensure the safe and economical design of structures built inside and above rock masses (Wu and Kulatilake 2012). In addition, the strength and deformability of rock masses are also important mechanical parameters in the analysis of rock mass engineering problems. Thus, the representative properties, including the uniaxial compressive strength (UCS) and deformation modulus (E_0), are taken as the parameters for mechanical RVE determination.

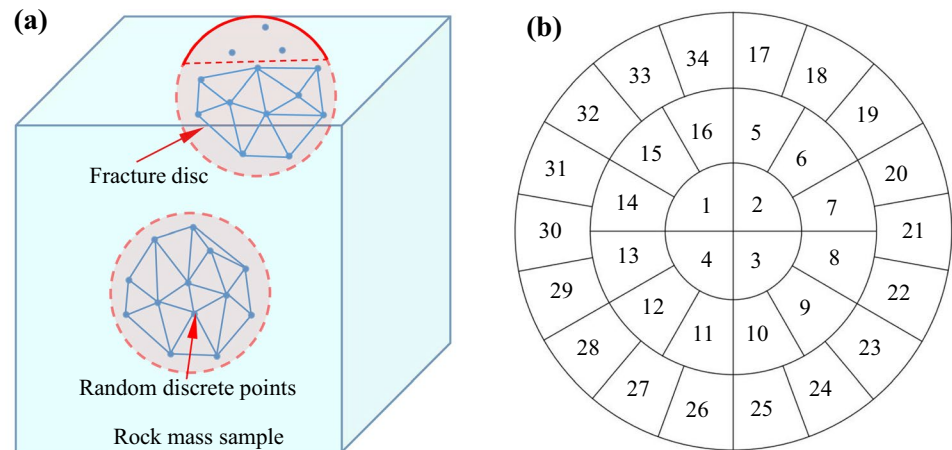
3.2 Parameter Determination Methods

Parameter values need to be accurately determined for use in RVE studies. Different calculation methods and measurement approaches are applied to various parameters as follows.

3.2.1 Geometrical Parameters

P_{32} (m^2/m^3) is the fracture area per rock mass volume, indicating that the value of this parameter comprehensively depends on fracture density and size. The Delaunay triangulation method is used to determine the P_{32} value (Zhang et al. 2017a),

Fig. 8 Determination methods of the geometrical parameters: (a) Delaunay triangulation method and (b) equal-area Schmidt projection diagram



as shown in Fig. 8a. Many random discrete points on the fracture disc are generated. Subsequently, Delaunay triangulation is applied to the points inside the sample to form triangles (Lee and Schachter 1980). The fracture area inside the sample is calculated by summing the triangle areas based on Heron's formula (Mitchell 2009). The areas of all the fractures inside the sample are summed and then divided by the sample volume to determine the P_{32} value.

The equal-area Schmidt projection diagram is divided into 34 equal-area patches, as shown in Fig. 8b. A fracture with an individual orientation can be projected into a corresponding patch. By repeating this procedure for all the fractures in a sample, the orientation frequencies of the fractures in the 34 patches can be determined. These 34 frequencies are treated as a 34-dimensional vector $\vec{A} (p_1, p_2, p_3, \dots, p_{34})$. Subsequently, the norm of vector $|\vec{A}|$ can be calculated, as shown in Eq. (3). The norm is a parameter value representing the orientation distribution information of the fractures, and it is called the orientation vector norm (A_{34}) in the subsequent sections.

$$A_{34} = |\vec{A}| = \sqrt{\sum_{n=1}^{34} p_n^2}. \quad (3)$$

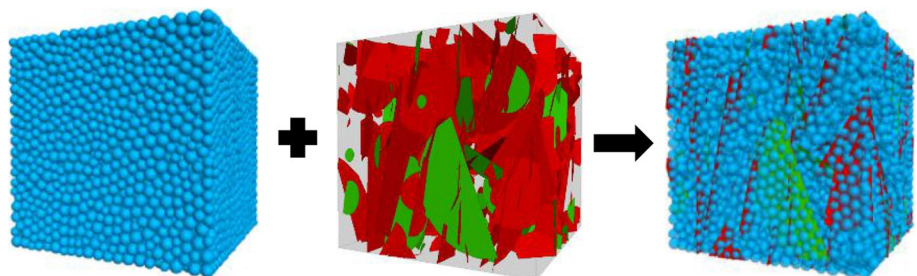
3.2.2 Mechanical Parameters

Only a sufficient quantity of samples that can accommodate the enough fractures can be used to derive the mechanical characteristics of rock masses. However, this kind of sample cannot be tested in the laboratory due to the difficulty of constructing such samples and the high economic cost. Therefore, a numerical simulation test is employed as the primary approach for obtaining the parameters.

The studied rock mass contains many non-penetration fractures. A recently reported method called the equivalent rock mass technique is suitable for simulating this kind of rock mass (Esmaili et al. 2010). With three-dimensional Particle Flow Code (PFC3D) software, a bonded particle model is constructed to simulate intact rock. Subsequently, an assembly of fractures is inserted into an intact rock to simulate rock mass, as shown in Fig. 9. By assigning the corresponding contact constitutive model to the particles near the fractures, the mechanical behaviour of fractures is well simulated.

In PFC3D, the spherical particle is the basic unit of rock mass. The particle and the contact model between particles need to be assigned parameters, i.e. micro-parameters. The mechanical behaviours and properties of the materials are controlled by their assigned micro-parameters. The rock is assigned the Parallel Bond contact model, providing the mechanical behaviour of a finite-sized piece of cement-like

Fig. 9 Equivalent rock mass technique in PFC3D



material deposited between the two contacting pieces. The structural plane is assigned the Smooth Joint contact model, providing the macroscopic behaviour of a linear elastic and either bonded or frictional interface with dilation. However, micro-parameters cannot be directly determined by laboratory or in situ tests (Yang et al. 2014). Following the principles of PFC3D, the micro-parameters first need to be calibrated. Specifically, a set of micro-parameters is assumed, and numerical tests are conducted. Subsequently, the macro-mechanical parameters are obtained and compared with those obtained in the laboratory or in situ test. If the parameters are inconsistent, the micro-parameters need to be changed (i.e. trial and error method) (Lee and Jeon 2011; Cao et al. 2016a, 2016b; Cheng et al. 2016).

The compression test of the rock and direct shear test of a structural plane are carried out in the calibration process. In the laboratory tests, the axial loading of the compression

tests is controlled by displacement, at a loading rate of 0.04 mm/min. The horizontal shearing of direct shear tests is also controlled by displacement, at a loading rate of approximately 0.5 mm/min. As shown in Fig. 10, the numerical tests used in the calibration are presented. In the compression numerical tests, the top and bottom walls are set as loading plates with a fixed speed. In the uniaxial compression tests, the sidewall is removed to simulate the unconfined state. In the triaxial compression tests, the sidewall is applied with the servo mechanism to apply the confining pressure. In the direct shear tests, the top and bottom walls are applied with the servo mechanism to apply the normal stress. The sidewalls are divided into upper and lower parts. The upper sidewalls are immobile. The lower sidewalls are moved horizontally with a fixed speed to apply the shear stress. In the numerical PFC3D tests, the calculation is run based on an explicit time stepping algorithm. The time step of each calculation is extremely small (1e-6 s). If the loading rate of the laboratory test is applied in the numerical test, it takes too long to calculate. Based on the previous studies, the loading rate is reasonably increased. The loading rate is set as 0.05 m/s in the compression test (Zhang et al. 2016, 2017b) and 0.1 m/s in the direct shear test (Bahaaddini et al. 2013, 2017; Xu et al. 2015a, 2015b).

Based on the relationship between the micro- and macro-parameters, the micro-parameters of the rock and fracture are determined by the trial and error method (Cundall and Potyondy 2004; Yang et al. 2006; Koyama and Jing 2007; Yoon 2007). The stress-strain curve of the uniaxial compression test is shown in Fig. 11a. Due to the limitation of the direct shear testing equipment, the shear strength and the shear displacement under shear strength are only recorded. The shear strengths are shown in Fig. 11b. The macro-mechanical parameters in the laboratory and numerical tests are shown in Table 4 (the mechanical parameter values

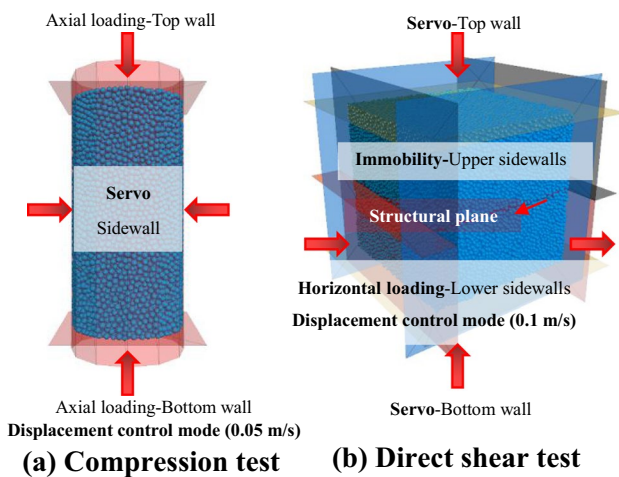


Fig. 10 The models of the numerical tests used in the calibration

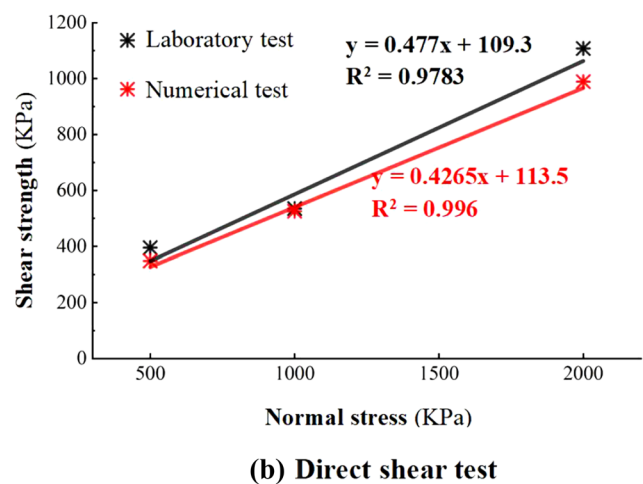
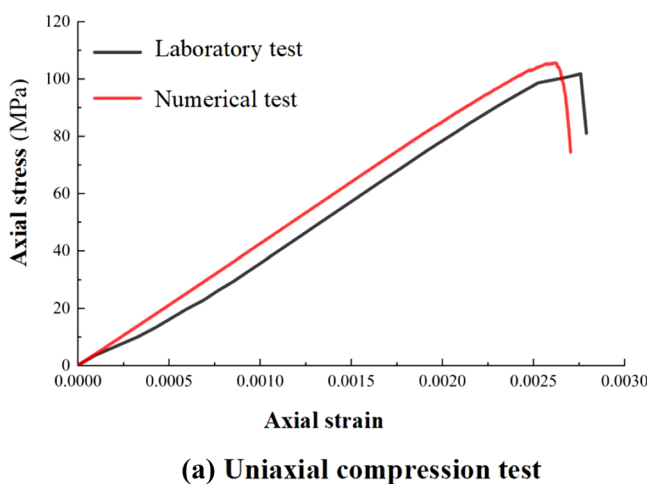


Fig. 11 The results of the laboratory and numerical tests

obtained from the laboratory parallel tests are presented in Table 1 in the supplementary data). The mechanical behaviours and parameters are roughly the same in the laboratory and numerical tests. The corresponding micro-parameters are shown in Table 5.

The rock mass model is extremely large, indicating that the number of particles will be too large for calculation if the calibrated particle radius (minimum radius of 0.15 mm) is used. For example, 2.06 million particles are generated in a sample with a side length of 10 m. Therefore, the particle radius needs to be appropriately enlarged. Studies have shown that when the number of particles in

the minimum side length of the model (RES) is equal to or larger than 10 (Eq. (4)), the number and radius of particles have a negligible effect on the macro-mechanical parameters (Deisman et al. 2008; Zhou et al. 2011). Table 6 shows the minimum particle radius, RES index and particle number in the samples with different side lengths after the enlargement of the particle.

$$RES = (L_{min}/R_{min}) \times [1/(1 + R_{max}/R_{min})], \quad (4)$$

where L_{min} is the minimum side length of the model, and R_{max} and R_{min} are the maximum and minimum particle radii, respectively.

Table 4 Comparison between the laboratory and numerical results

	Macro-parameters	Laboratory results	Numerical results
Compression test	Uniaxial compressive strength (MPa)	101.8	105.6
	Young's modulus (GPa)	42.6	40.3
	Poisson's ratio	0.22	0.20
	Cohesion (MPa)	28.8	30.1
	Internal friction angle (°)	34.0	31.8
Direct shear test	Cohesion (KPa)	109.3	113.5
	Internal friction angle (°)	25.5	23.1

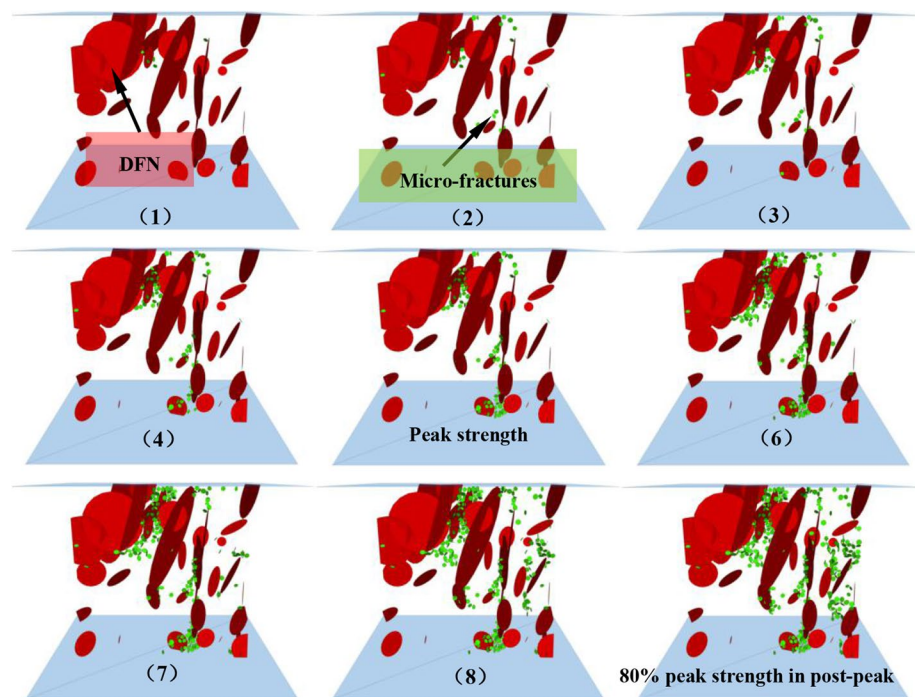
Table 5 Micro-parameters of the rock and fractures in PFC3D

	Micro-parameters	Values	Remarks
Particle	Minimum radius (mm)	0.15	Uniform distribution
	R_{max} / R_{min}	1.5	
	Particle density (kg / m ³)	2940	
	Particle friction coefficient	1.0	
	Particle normal / shear stiffness	1.5	
	Particle effective modulus (GPa)	16	
Parallel-bond contact model	Parallel-bond radius multiplier	1.0	Normal distribution
	Parallel-bond normal / shear stiffness	1.5	
	Parallel-bond effective modulus (Gpa)	16	
	Parallel-bond normal strengths, mean (MPa)	15	
	Parallel-bond normal strength, SD (MPa)	3	
	Parallel-bond shear strengths, mean (MPa)	22	
Fracture	Parallel-bond shear strength, SD (MPa)	4.4	20% of mean value
	Joint particle normal stiffness (N / m)	20e9	
	Joint particle shear stiffness (N / m)	20e9	
	Joint particle friction coefficient	0.5	
Dilation angle (°)	0		

Table 6 Particle size information of samples with different side lengths

Sample side length (m)	6	8	10	12	14	16	18	20	22
R_{min} (m)	0.15	0.15	0.22	0.22	0.22	0.22	0.25	0.25	0.25
RES	16	21	18	22	25	29	29	32	35
Particle number	6325	15,011	9079	15,682	24,895	37,167	35,636	48,842	67,349

Fig. 12 Propagation process of micro-fractures for a filter in a sample with a side length of 10 m in uniaxial compression test



Uniaxial compression tests are run with the corresponding micro-parameters and particle radius. The UCS and E_0 values are recorded to determine the mechanical RVE. To ensure the correctness of the simulation, the fractures are monitored. Due to the limitation of the 3D perspective, a filter with a thickness of 1.5 m is presented to clearly show the micro-fractures. Figure 12 shows the propagation process of the micro-fractures. As shown in Fig. 12, the initial positions of the micro-fractures are located at the edge of the 3D fracture network. With the increase in axial stress, the micro-fractures gradually propagate, and the micro-fractures and the 3D fracture network coalesce. These phenomena are reasonable and consistent with the failure process of rock masses in laboratory tests (Cao et al. 2016a, 2016b).

3.3 Parameter Sampling

The space that accommodates the fracture network is constructed prior to the RVE determination. The edge effect denotes the small fracture density in the edge regions. Therefore, the 3D fracture networks generated in Sect. 2.3 should be reduced. In the present study, the sizes of the 3D fracture networks in the x , y , and z directions are separately reduced by twice the average trace length (Zhang et al. 2012). Eventually, 3D fracture networks with dimensions of $46\text{ m} \times 36\text{ m} \times 36\text{ m}$ are obtained for RVE determination.

Cubes with increasing side lengths (i.e. from 4 to 22 m) are sampled to analyse the size effects and determine the RVE sizes. The following three kinds of sampling methods are considered in the study of the RVE sizes:

(a) Traditional sampling method.

An arbitrary point is taken as a constant centre point. Subsequently, the cubes centred at this point with different side lengths are sampled (Fig. 13a).

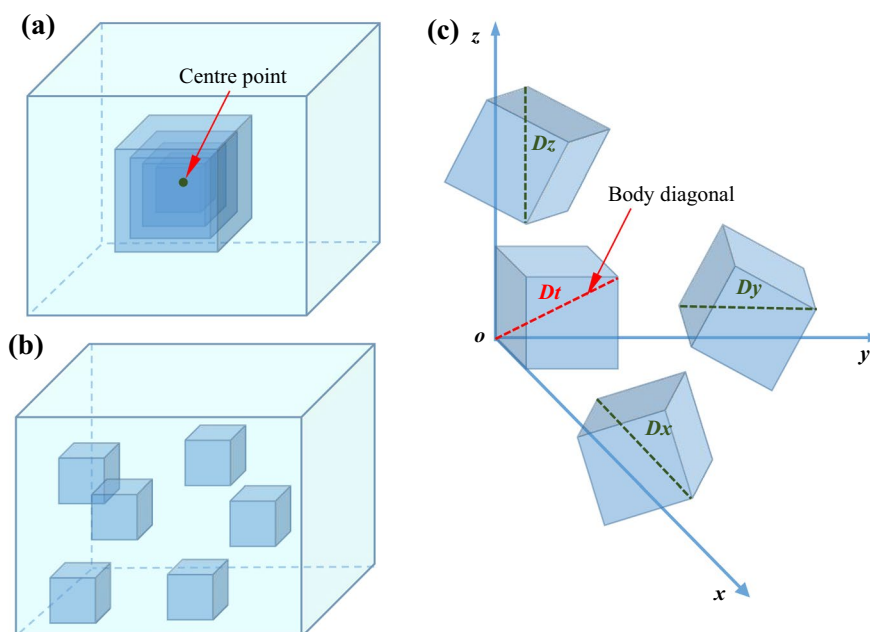
(b) Sampling method considering inhomogeneity.

The traditional sampling method assumes that the fractures are homogeneously distributed in rock masses. However, fractures in both natural rock masses and 3D fracture networks are typically inhomogeneous (Liu et al. 2018). Therefore, the corresponding RVE is characterised by spatial variability (Zhang et al. 2013a, b). This method is used to consider the spatial effect. Multiple cubes with a same side length but random centre points are sampled (Fig. 13b).

(c) Sampling method considering anisotropy.

The geometrical and mechanical properties of rock masses are characterised by anisotropy. Therefore, this method, in which the sampling direction is rotated multiple times on the basis of the sampling method considering inhomogeneity, is generated to study whether RVE has the directional variability, as shown in Fig. 13c. In the figure, Dt is the direction of the body diagonal in the samples with the conventional sampling direction. Dx , Dy and Dz are the directions of the body diagonal in the rotated samples. Cubes with different directions are sampled to determine the RVEs in different directions. Because these directions are very different, the anisotropy can be shown clearly.

Fig. 13 Different sampling methods: (a) traditional sampling method, (b) sampling method considering inhomogeneity and (c) sampling method considering anisotropy



3.4 Quantitative Methods of RVE Determination

In the traditional sampling method, an individual parameter value is determined for a given size. The rate of change in the parameter values (Eq. (5)) is used to determine the RVE size. When the rate of change is less than an acceptable value, the parameter is in a convergence state. The acceptable rate of change is chosen as 5% in this article. When the size is larger than the critical value, i.e. the RVE size, the rate of change will always be less than 5%.

$$\varepsilon = \left| \frac{k_i - k_{i-2}}{k_i} \right| \times 100\%, \quad (5)$$

where k_{i-2} and k_i are the parameter values of rock mass samples with sizes of $i-2$ m and i m, respectively, and ε is the rate of change in the parameter values.

In the sampling methods considering the inhomogeneity and anisotropy, twenty cubes with a same side length and direction but random centre points are sampled, as shown in Fig. 13. Thus, the main problem is how to quantify a comprehensive parameter for the twenty parameter values.

The coefficient of variation (CV), the ratio of the standard deviation to the mean value, is introduced to quantify the discreteness of the parameter values for the samples with a given size and direction. The parameter values have a significant discreteness under a large CV value. Different acceptable values of CV have been used to determine RVE size in previous studies (5%, 10%, 20%) (Min and Jing 2003; Esmaili et al. 2010). With the increase in the acceptable value of CV, the allowable discreteness of the parameter values under the RVE size gradually increases; thus, the RVE

size gradually decreases. For the different parameters in the RVE determination, the same acceptable value of CV should be used. We take a moderate value (10%) to determine the RVE size in this article.

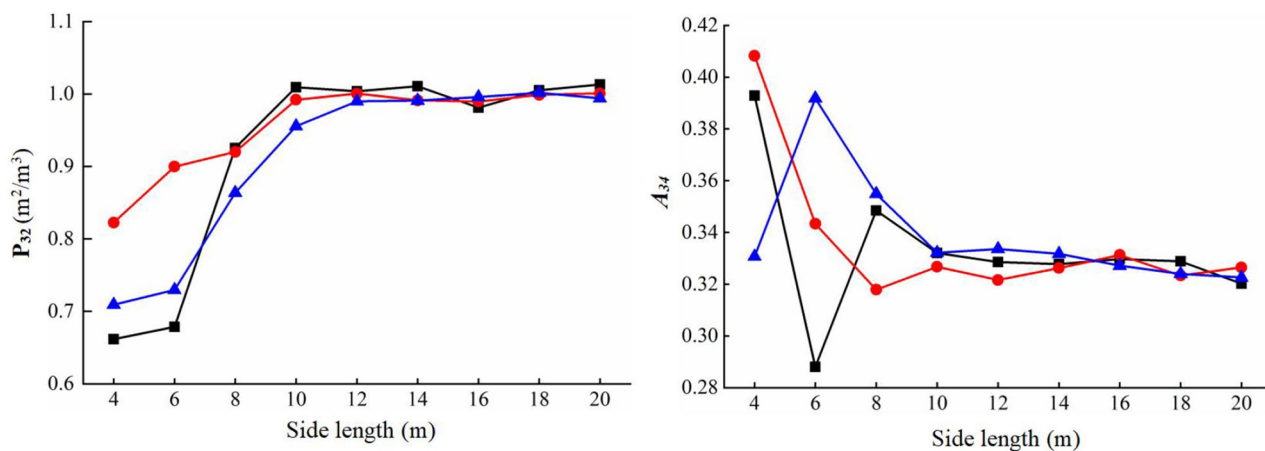
4 Determination of RVE with different considerations

4.1 Determination of RVE with the Traditional Method

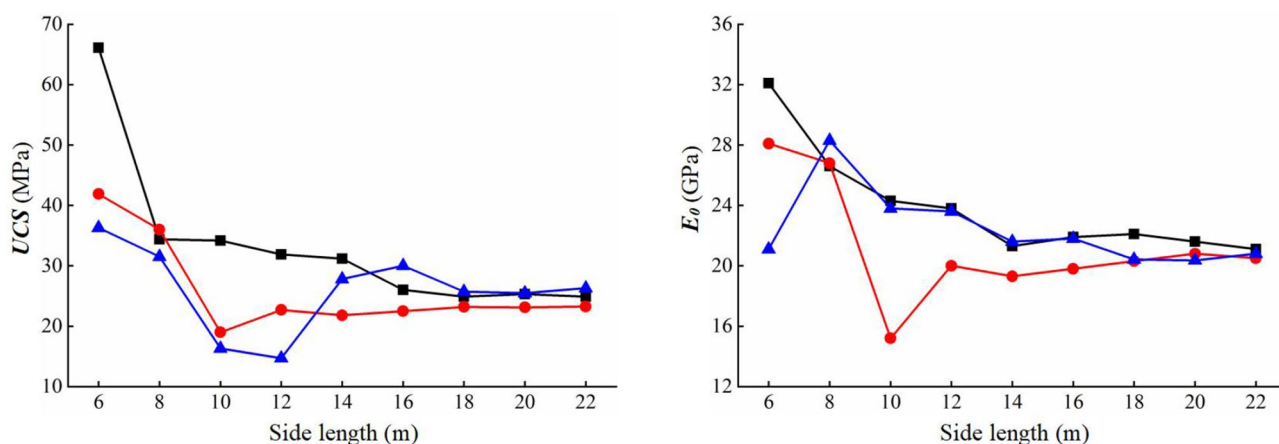
The traditional sampling method (Sect. 3.3a) is applied, and then the rate of change in the parameter values (Eq. (5)) is calculated to determine the RVE sizes. The following three centre points are taken to carry out this study: (15 m, 15 m, 15 m), (20 m, 20 m, 20 m), and (25 m, 25 m, 25 m).

The geometrical and mechanical parameter values are obtained using the method introduced in Sect. 3.2, and the results are shown in Fig. 14. Distinct size effects are observed. Overall, an increase in sample size gradually enlarges P_{32} and decreases A_{34} , UCS and E_0 . When the sample size is small, the parameter values fluctuate dramatically with size. The variability gradually weakens as the size increases.

The rate of change in the geometrical and mechanical parameter values are calculated, and then the RVE are determined based on the acceptable value of 5%. The larger value of RVE sizes based on P_{32} and A_{34} is taken as the geometrical RVE size. The larger value of RVE sizes based on UCS and E_0 is taken as the mechanical RVE size.



(a) Geometric parameters



(b) Mechanical parameters

Parameter values with different centre points —■— (15 m, 15 m, 15 m) —●— (20 m, 20 m, 20 m) —▲— (25 m, 25 m, 25 m)

Fig. 14 Geometrical and mechanical parameter values with different centre points

Table 7 RVE sizes in different locations with the traditional method

Region	RVE sizes					
	P_{32}	A_{34}	Geometrical RVE	UCS	E_0	Mechanical RVE
A	12 m	10 m	12 m	18 m	16 m	18 m
B	12 m	10 m	12 m	14 m	14 m	14 m
C	14 m	12 m	14 m	20 m	20 m	20 m

The results are shown in Table 7. Both the geometrical and mechanical RVEs vary among the study regions.

As illustrated in Fig. 14, the parameter values vary among the locations within 3D fracture networks, suggesting that the rock masses are characterised by inhomogeneity. Table 7 shows that the RVEs vary among the study regions, reflecting the spatial effect on RVE size.

Moreover, the spatial effect on the mechanical RVE is more significant than that on the geometrical RVE.

The above studies show the necessity of considering the inhomogeneity in RVE determination. Subsequently, we study whether considering the anisotropy is necessary. The parameter values in different directions with a centre point (15 m, 15 m, 15 m) are shown in Fig. 15, in which the

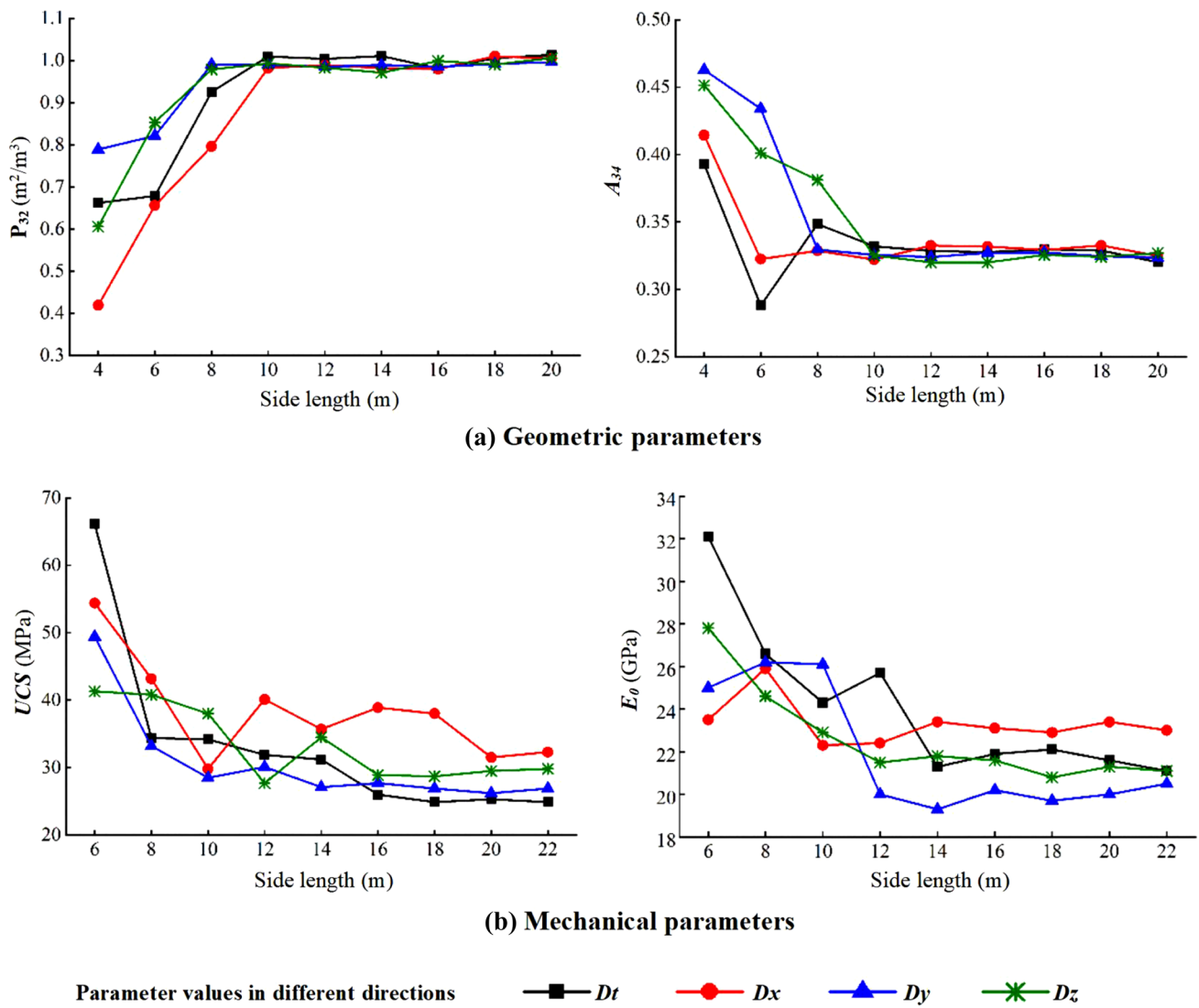


Fig. 15 Geometrical and mechanical parameter values in different directions

Table 8 RVE sizes in different directions determined with the traditional method

Direction	RVE sizes					
	P_{32}	A_{34}	Geometrical RVE	UCS	E_0	Mechanical RVE
D_t	12 m	10 m	12 m	18 m	16 m	18 m
D_x	12 m	8 m	12 m	22 m	12 m	22 m
D_y	10 m	10 m	10 m	16 m	14 m	16 m
D_z	10 m	12 m	12 m	18 m	14 m	18 m

directions are shown in Fig. 13c. The anisotropies of the geometrical and mechanical parameters are distinct. Furthermore, the RVE sizes vary among the directions, as shown in Table 8.

The above studies indicate that the traditional method needs to be improved, as it can only represent a single

study region and direction. In the subsequent sections, the RVEs are subjected to an in-depth study by considering the special natures of the rock masses.

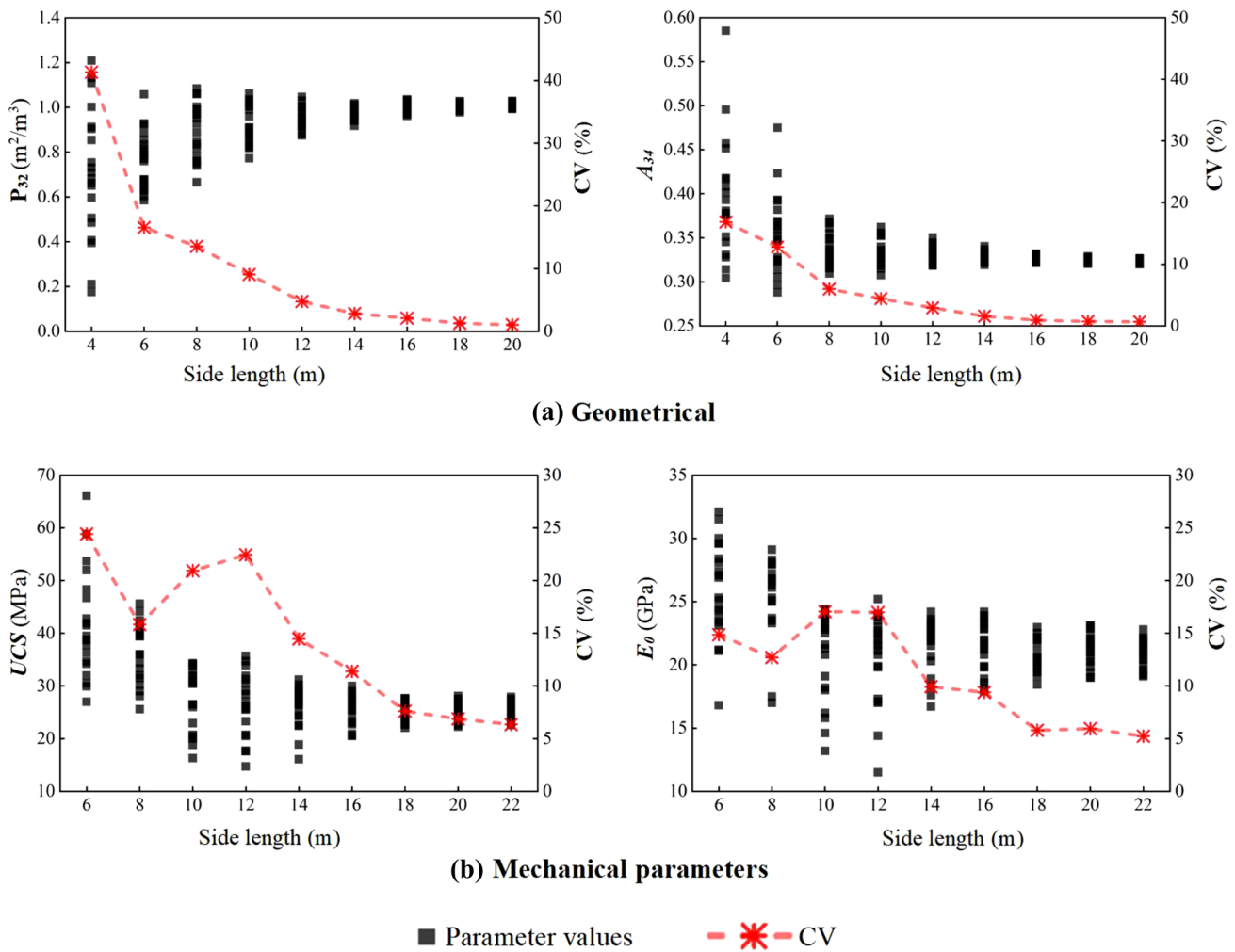


Fig. 16 Geometrical and mechanical parameter values and CV values in random locations

4.2 Determination of RVE with the Consideration of Inhomogeneity

The sampling method considering the inhomogeneity is used to study the geometrical and mechanical RVEs (Fig. 13b). An acceptable CV value is used to determine the RVE sizes.

The geometrical and mechanical parameter values are calculated, as shown in Fig. 16. The variability in the parameter values of the samples with a same size is shown, which corresponds to the inhomogeneity of the fracture structures. When the sample size is small, the parameter values vary significantly with location. With the increase in the sample size, the difference in the fracture structures between the samples gradually weakens. Thus, the variability in the parameter values gradually weakens, i.e. the CV gradually

decreases. All of the studied parameters exhibit the aforementioned trends.

The CV curves of the geometrical parameters are regular. Thus, the CV curves of the mechanical parameters that are relatively irregular are emphasised. When the sample size is small, the failure of a sample is likely to depend on a minority of fractures that play a key role in the mechanical behaviour. Thus, the mechanical properties are extremely inhomogeneous, which leads to the irregularity of the CV curve at small sample sizes. This irregularity indicates that the mechanical RVE is larger than the geometrical RVE.

As shown in Fig. 16, the CV varies among the parameters. Overall, the CVs of the mechanical parameters are larger than those of the geometrical parameters. This

indicates that the inhomogeneity of the mechanical properties is more significant. Based on the acceptable CV value of 10%, the RVE sizes based on P_{32} and A_{34} are 10 m and 8 m, respectively. The larger value of 10 m is taken as the geometrical RVE size. The RVE sizes based on UCS and E_0 are 18 m and 14 m, respectively. Similarly, the mechanical RVE size is 18 m, which is far larger than the geometrical RVE.

4.3 Determination of RVE with the Consideration of Anisotropy

On the basis of the sampling method considering the anisotropy (Fig. 13c), the RVEs in the different directions are determined by analysing the CV. This method simultaneously considers the inhomogeneity and anisotropy of the rock masses.

The geometrical and mechanical parameter values are determined in different directions, as shown in Fig. 17. The anisotropies of the rock mass properties are observed (Sect. 4.1). Thus, we mainly discuss the anisotropy characteristics of the different parameters. For the geometrical parameters, when the sample size is sufficiently large (16 m), the parameter values in the different directions are nearly the same. However, for the mechanical parameters, the anisotropy is obvious within the entire sizes. In particular, UCS and E_0 in the Dx direction are larger than those in the other directions. Therefore, the anisotropy of the mechanical properties is more significant than that of the geometrical properties.

As shown in Fig. 17, the CV varies with direction, that is, the size effects are anisotropic. Furthermore, the degrees of anisotropy in the size effects are different with parameter. Based on the previous studies on the quantification of anisotropy, the anisotropy of size effects is measured quantitatively by the anisotropy coefficient A_p (Eq. (6)) (Il'Chenko and Gannibal 2019). Figure 18 shows the A_p values of the CV of the different parameters. Overall, the A_p values of the mechanical parameters are larger than those of the geometrical parameters. Therefore, the size effects of the mechanical parameters have a more significant anisotropy than those of the geometrical parameters. Furthermore, that of P_{32} is relatively weak.

$$A_p = \frac{1}{CV_m} \sqrt{(CV_t - CV_m)^2 + (CV_x - CV_m)^2 + (CV_y - CV_m)^2 + (CV_z - CV_m)^2}, \tag{6}$$

where CV_t , CV_x , CV_y and CV_z are the values of CV in the Dt , Dx , Dy and Dz directions,

$CV_m = (CV_t + CV_x + CV_y + CV_z)/4$ is the average value of CV in the different directions.

The RVE sizes in different directions are determined using a CV value of 10%, as shown in Table 9. The results

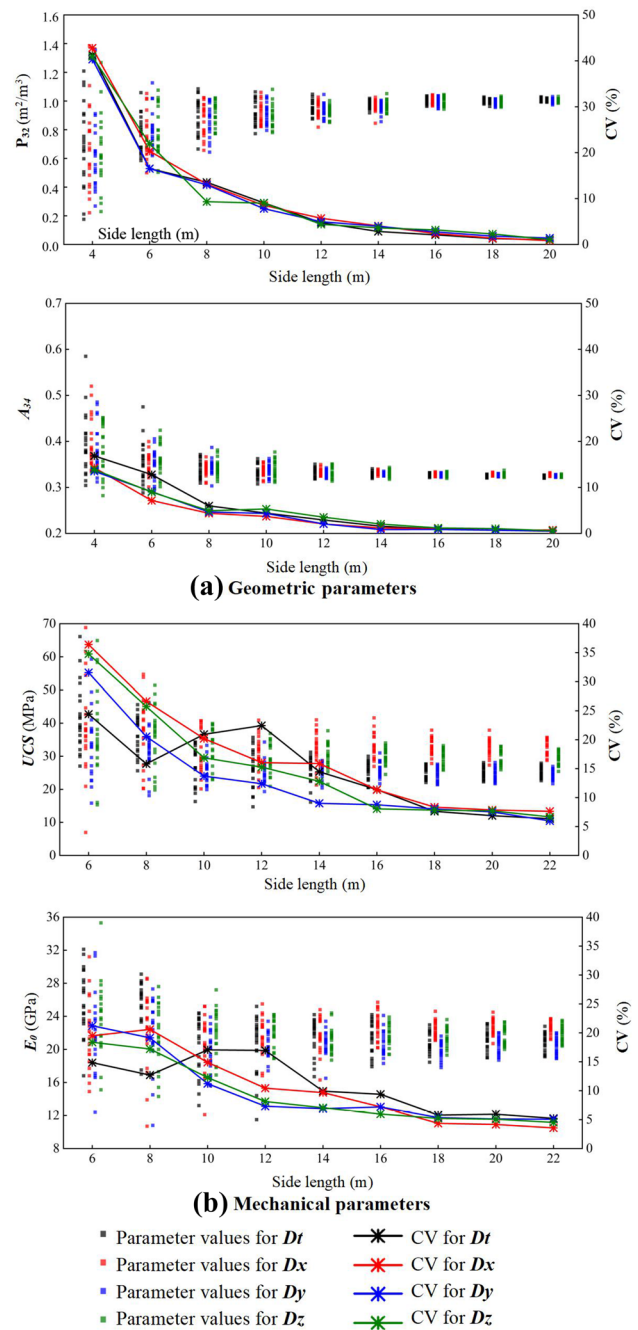


Fig. 17 Geometrical and mechanical parameter values and CV values in different directions

show that the RVE size has a directional effect. Furthermore, the directional effect on the mechanical RVE is more significant than that on the geometrical RVE, which is consistent with the analysis of the anisotropy degrees of the size effects of different parameters. In particular, based on the mechanical parameters, the RVE sizes in the Dy directions are smaller than those in the other directions. The directional effect on the geometrical RVE is not very obvious.

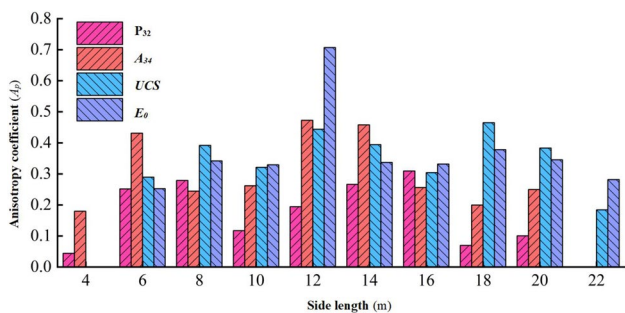


Fig. 18 The anisotropy coefficient values (A_p) of the CVs of different parameters

In this study, we take the maximum of the RVE sizes in different directions as the final RVE size. The geometrical and mechanical RVE sizes are 10 and 18 m, respectively. As reported in Table 9, for the rock masses in the present study, the RVE sizes in the D_t direction are largest; thus, there are no changes in the RVE sizes under anisotropy consideration. Through the above studies, the directional effect on the RVE is verified. Therefore, the consideration of anisotropy is necessary to improve the accuracy of RVE determination.

5 Comparison between geometrical and mechanical RVE sizes

We discuss the relationship between the geometrical and mechanical RVE sizes in this section. Many studies have shown that the size effects of the various properties of rock masses are mainly caused by the complex fracture structures (Piggott and Elsworth 1989; Zhang and Einstein 2000; Harrison et al. 2002; Fereshtenejad et al. 2016; Ni et al. 2016). Therefore, the geometrical features theoretically control the mechanical features. In the analysis of Zhang et al. (2013b), fractures were found to be the key factors controlling rock mass characteristics. These studies indirectly show that RVEs based on the fracture characteristics are representative, have universality, and can, thus, reflect the size effects of mechanical properties; that is, the geometrical RVE is

larger than the mechanical RVE for the same rock masses. However, in the RVE determination of practical engineering rock masses, the mechanical RVE is larger than the geometrical RVE. For example, Esmaili et al. (2010) found that the mechanical RVE (7 m × 7 m × 14 m) is larger than the geometrical RVE (3.5 m × 3.5 m × 7 m). In this study, the mechanical RVE (18 m × 18 m × 18 m) is also larger than the geometrical RVE (10 m × 10 m × 10 m).

Given the complexity of the mechanical properties of rock masses, the conclusion regarding the relationship between geometrical and mechanical RVE sizes cannot be easily concluded. In this article, the studies involving the mechanical aspect all focus on unconfined rock masses. The confining pressure has a great influence on the mechanical characteristics of rock masses (Yao et al. 2019; Guo et al. 2020). Therefore, we conjecture that the relationship between geometrical and mechanical RVE sizes may be influenced by confining pressure. More importantly, rock masses work under the three-dimensional stress states in engineering.

A study on the influence of confining pressure on mechanical RVE size is undertaken, and then the mechanical RVE considering the confining pressure is compared with the geometrical RVE. We separately take five samples with sizes of 8 m, 10 m and 12 m to run the triaxial compression test. Confining pressures of 1 MPa, 3 MPa, 5 MPa, 7 MPa, 10 MPa and 15 MPa are applied.

The shear strength and E_0 values are recorded, and then the CVs are calculated, as shown in Fig. 19 (the stress–strain curves of the samples with different sizes under different confining pressures are presented in Fig. 1 in the supplementary data). With the increase in the confining pressure, the shear strength gradually increases, but the law of E_0 is not clear. The CVs of the shear strength and E_0 gradually decrease as the confining pressure increases. When the confining pressure is less than or equal to 5 MPa, the CVs of the mechanical parameters are larger than 10%. When the confining pressure is equal to 7 MPa, the CVs of the mechanical parameters with sample sizes of 10 m and 12 m are less than 10%. When the confining pressure is greater than or equal to 10 MPa, the CVs of the mechanical parameters are less than 10%. Therefore, the mechanical RVE size under a confining pressure of 7 MPa is the same as the corresponding geometrical RVE size, and the mechanical RVE size under a

Table 9 Geometrical and mechanical RVE sizes in different directions

Direction	RVE sizes					
	P_{32}	A_{34}	Geometrical RVE	UCS	E_0	Mechanical RVE
D_t	10 m	8 m	10 m	18 m	14 m	18 m
D_x	10 m	6 m	10 m	18 m	14 m	18 m
D_y	10 m	6 m	10 m	14 m	12 m	14 m
D_z	8 m	6 m	8 m	16 m	12 m	16 m

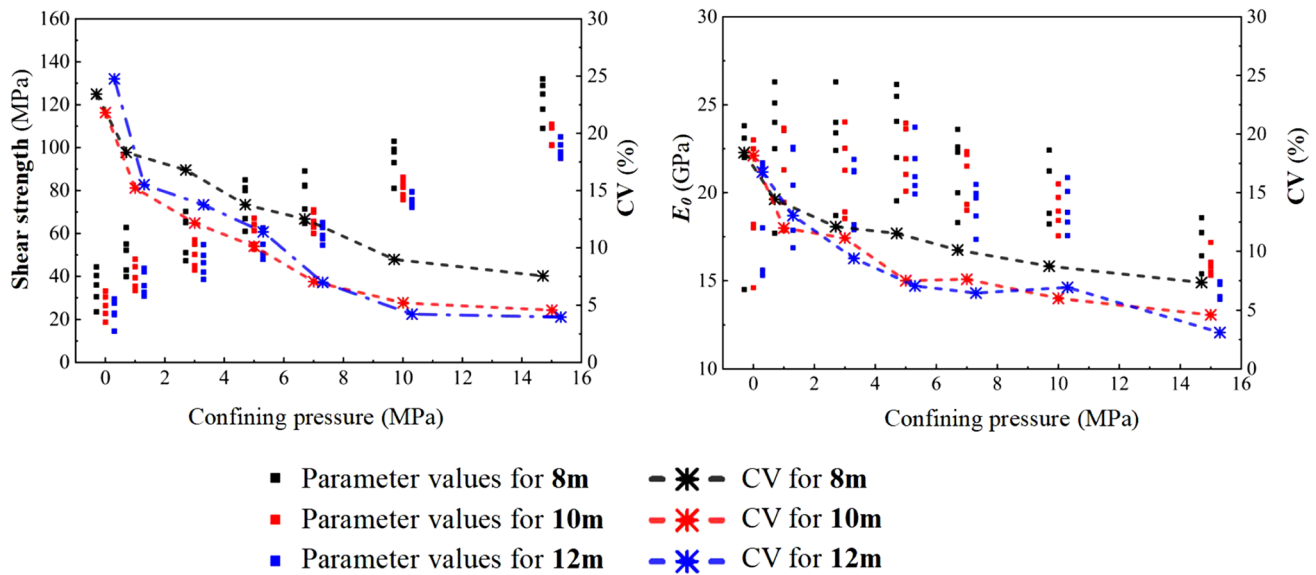


Fig. 19 Parameter values and CV values with increasing confining pressure

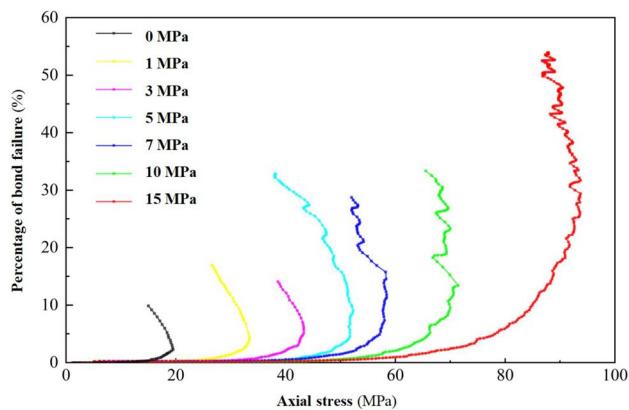


Fig. 20 The changes in the percentage of bond failure under different confining pressures during the compression test

high confining pressure (greater than or equal to 10 MPa) is smaller than the corresponding geometrical RVE size.

During the compression tests, the percentage of bond failure is recorded. The changes in the percentage of bond failure with the increase in the axial stress in the sample with a size of 10 m are shown in Fig. 20. With increasing confining pressure, the initiation stress of micro-fractures gradually increases, and the percentage of bond failure gradually decreases under the same axial stress. This indicates that the confining pressure limits the generation and propagation of micro-fractures. The influence of fracture structures on the mechanical properties gradually weakens as the confining pressure increases. Therefore, the mechanical RVE size gradually decreases.

6 Discussion

The calculation results of the RVE size at the sluice show that the equivalent continuum model is applicable for large-scale rock mass engineering problems such as stability analysis of the entire sluice. In this case, the mechanical parameters obtained from samples with the RVE size are representative and can be used as the input parameters of the model. On the other hand, for the small-scale excavation of rock masses, the equivalent rock mass technique used in this article is applicable for rock masses characterised by non-persistent fractures.

The consideration of anisotropy is necessary in practical problems. For some engineering problems with directional features, the direction in the RVE determination should be consistent with that involved in the engineering. The parameter values in the corresponding direction are obtained for the RVE determination to improve the accuracy and efficiency. In some engineering, the geometrical or mechanical characteristics in various directions are related to the problem of analysis. We can determine the RVEs in several very different directions, such as the directions selected in this study. Subsequently, the maximum is taken as the final RVE size to ensure accuracy. For the study object of the rock masses in the dam foundation of the sluice, stability analysis is a crucial engineering problem. Instability may occur in multiple directions. Therefore, the maximum of the RVE sizes in different directions is taken as the final RVE size.

Mechanical tests are necessary in the determination of the mechanical RVE, which is more complex and time-consuming than the determination of the geometrical RVE. To quickly determine or roughly estimate the mechanical RVE for the

analysis of rock mass engineering problems, it is necessary to study the relationship between the geometrical and mechanical RVEs. The present study shows that the mechanical RVE without confining pressure is almost twice the geometrical RVE. With increasing confining pressure, the mechanical RVE gradually decreases. In practical engineering, rock masses work under the ground stresses, which are not fixed. Therefore, the mechanical RVE determined without confining pressure is sufficient and reasonable for the analysis of engineering problems. Future developments will be aided by the quantitative determination of the relationship between geometrical and mechanical RVEs to improve the efficiency of solving engineering problems.

7 Conclusion

The rock masses downstream of the sluice gate of the Datengxia Hydropower Station are taken as the study area to determine the geometrical and mechanical RVEs by focusing on the special natures (inhomogeneity and anisotropy) of the rock masses. The volumetric fracture density (P_{32}) and orientation vector norm (A_{34}) are taken to comprehensively characterise the complex fracture structures. The uniaxial compressive strength (UCS) and deformation modulus (E_0) obtained by PFC3D are taken to present the mechanical characteristics. The conclusions can be summarised as follows:

- 1 Based on the sampling methods considering the special natures, the results indicate that the special natures of mechanical properties are more significant than those of geometrical properties.
- 2 The inhomogeneity of rock masses results in the RVE sizes varying with location, i.e. spatial effect on RVE sizes. The anisotropy of rock masses results in the RVE sizes varying with direction, i.e. directional effect on RVE sizes. Furthermore, these effects are more significant on the mechanical properties than on the geometrical properties. Therefore, the traditional method of RVE determination needs to be improved.
- 3 Considering the special natures of the studied rock masses, the RVEs are determined by using an acceptable CV value of 10%. The mechanical RVE size is 18 m, which is far larger than the geometrical RVE size of 10 m. The confining pressure has an influence on the mechanical RVE size. The mechanical RVE size gradually decreases as the confining pressure increases. When the confining pressure is high enough (greater than or equal to 10 MPa), the mechanical RVE is smaller than the geometrical RVE.

Acknowledgements This work was financially supported by the National Key Research and Development program of China [grant number: 2019YFA0705504] and the National Nature Science Foundation of China [grant numbers: 42022053; 41877220; U1702241; 41702301].

Declarations

Conflict of interest The authors declare that they have no known competing financial interests or personal relationships that could have appeared to influence the work reported in this paper.

References

- Abrah B, Karami M, Faramarzi L (2011) Importance of anisotropy in dam foundation, estimated by in-situ dilatometer tests. In: Proceedings of the 12th ISRM international congress on rock mechanics, Beijing, China 1857–1860. <https://doi.org/10.1201/b11646-352>
- Bahaaddini M (2017) Effect of boundary condition on the shear behaviour of rock joints in the direct shear test. *Rock Mech Rock Eng* 50(5):1141–1155. <https://doi.org/10.1007/s00603-016-1157-z>
- Bahaaddini M, Sharrock G, Hebblewhite BK (2013) Numerical direct shear tests to model the shear behaviour of rock joints. *Comput Geotech* 51:101–115. <https://doi.org/10.1016/j.compgeo.2013.02.003>
- Bear J (1972) Dynamics of fluids in porous media. American Elsevier, New York
- Billaux D, Chiles JP, Hestir K, Long J (1989) Three-dimensional statistical modelling of a fractured rock mass—an example from the Fanay-Augères mine. *Int J Rock Mech Min Sci* 26(3–4):281–299. [https://doi.org/10.1016/0148-9062\(89\)91977-3](https://doi.org/10.1016/0148-9062(89)91977-3)
- Bryant FB, Satorra A (2012) Principles and practice of scaled difference chi-square testing. *Struct Equ Model* 19(3):372–398. <https://doi.org/10.1080/10705511.2012.687671>
- Cao RH, Cao P, Fan X, Xiong XG, Lin H (2016a) An experimental and numerical study on mechanical behavior of ubiquitous-joint brittle rock-like specimens under uniaxial compression. *Rock Mech Rock Eng* 11(49):4319–4338. <https://doi.org/10.1007/s00603-016-1029-6>
- Cao RH, Cao P, Lin H, Pu CZ, Ou K (2016b) Mechanical behavior of brittle rock-like specimens with pre-existing fissures under uniaxial loading: experimental studies and particle mechanics approach. *Rock Mech Rock Eng* 49(3):763–783. <https://doi.org/10.1007/s00603-015-0779-x>
- Castelli M, Saetta V, Scavia C (2003) Numerical study of scale effects on the stiffness modulus of rock masses. *Int J Geomech* 3(2):160–169. [https://doi.org/10.1061/\(ASCE\)1532-3641\(2003\)3:2\(160\)](https://doi.org/10.1061/(ASCE)1532-3641(2003)3:2(160))
- Chen DH, Chen HE, Zhang W, Tan C, Ma ZF, Chen JP, Shan B (2020) Buckling failure mechanism of a rock dam foundation fractured by gentle through-going and steep structural discontinuities. *Sustainability* 12(13):5426. <https://doi.org/10.3390/su12135426>
- Cheng C, Chen X, Zhang SF (2016) Multi-peak deformation behavior of jointed rock mass under uniaxial compression: insight from particle flow modeling. *Eng Geol* 213:25–45. <https://doi.org/10.1016/j.enggeo.2016.08.010>
- Cundall PA, Potyondy DO (2004) A bonded-particle model for rock. *Int J Rock Mech Min Sci* 41(8):1329–1364. <https://doi.org/10.1016/j.ijrmms.2004.09.011>
- Deisman N, Ivars DM, Pierce M (2008) PFC2D Smooth joint contact model numerical experiments. In: Proceedings of GeoEdmonton'08, Edmonton, Canada 83–87

- Esmaili K, Hadjigeorgiou J, Grenon M (2010) Estimating geometrical and mechanical REV based on synthetic rock mass models at Brunswick Mine. *Int J Rock Mech Min Sci* 47(6):915–926. <https://doi.org/10.1016/j.ijrmmms.2010.05.010>
- Fereshtenejad S, Afshari MK, Bafghi AY, Laderian A, Safaei H, Song JJ (2016) A discrete fracture network model for geometrical modeling of cylindrically folded rock layers. *Eng Geol* 215:81–90. <https://doi.org/10.1016/j.enggeo.2016.11.004>
- Guo SF, Qi SW, Zhan ZF, Ma L, Gure EG, Zhang SS (2020) Numerical study on the progressive failure of heterogeneous geomaterials under varied confining stresses. *Eng Geol* 269:105556. <https://doi.org/10.1016/j.enggeo.2020.105556>
- Harrison J, Hudson J, Popescu M (2002) Engineering rock mechanics: Part 2. illustrative worked examples. *Appl Mech Rev* 55(2): B30–B31. <https://doi.org/10.1115/1.1451166>
- Il'Chenko VL, Gannibal MA (2019) Elastic anisotropy and internal structure of rocks from the uranium ore occurrences of the Litsa Ore Area (Kola Region, Russia). *Geosciences* 9(7):284. <https://doi.org/10.3390/geosciences9070284>
- Ivars DM, Pierce M, DeGagnè D, Darcel C (2008) Anisotropy and scale dependency in jointed rock-mass strength—A synthetic rock mass study. In: *Proceedings of the 1st international FLAC/DEM symposium on numerical modeling*, Minneapolis, USA 231–239.
- Koyama T, Jing L (2007) Effects of model scale and particle size on micro-mechanical properties and failure processes of rocks—a particle mechanics approach. *Eng Anal Bound Elem* 31(5):458–472. <https://doi.org/10.1016/jenganabound.2006.11.009>
- Kulatilake PHSW (1985) Estimating elastic constants and strength of discontinuous rock. *J Geotech Eng* 111(7):847–864. [https://doi.org/10.1061/\(ASCE\)0733-9410\(1985\)111:7\(847\)](https://doi.org/10.1061/(ASCE)0733-9410(1985)111:7(847))
- Kulatilake PHSW, Wu TH (1984) Estimation of mean trace length of discontinuities. *Rock Mech Rock Eng* 17(4):215–232. <https://doi.org/10.1007/BF01032335>
- Lee H, Jeon S (2011) An experimental and numerical study of fracture coalescence in pre-cracked specimens under uniaxial compression. *Int J Solids Struct* 48(6):979–999. <https://doi.org/10.1016/j.ijsolstr.2010.12.001>
- Lee DT, Schachter BJ (1980) Two algorithms for constructing a Delaunay triangulation. *Int J Parallel Prog* 9(3):219–242. <https://doi.org/10.1007/BF00977785>
- Li YY, Chen JP, Shang YJ (2017) Determination of the geometrical REV based on fracture connectivity: a case study of an underground excavation at the Songta dam site. *China B Eng Geol Environ* 77(4):1599–1606. <https://doi.org/10.1007/s10064-017-1063-y>
- Li KQ, Li DQ, Liu Y (2020) Meso-scale investigations on the effective thermal conductivity of multi-phase materials using the finite element method. *Int J Heat Mass Tran* 151:119383. <https://doi.org/10.1016/j.jheatmasstransfer.2020.119383>
- Liu Y, Wang Q, Chen JP, Song SY, Zhan JW, Han XD (2018) Determination of geometrical REV based on volumetric fracture intensity and statistical tests. *Appl Sci* 8(5):800. <https://doi.org/10.3390/app8050800>
- Min KB, Jing L (2003) Numerical determination of the equivalent elastic compliance tensor for fractured rock masses using the distinct element method. *Int J Rock Mech Min Sci* 40(6):795–816. [https://doi.org/10.1016/S1365-1609\(03\)00038-8](https://doi.org/10.1016/S1365-1609(03)00038-8)
- Mitchell DW (2009) 93.10 A heron-type area formula in terms of sines. *Math Gaz* 93(526):108–109. <https://doi.org/10.1017/S00255572018430X>
- Ni PP, Wang SH, Wang CG, Zhang SM (2016) Estimation of REV size for fractured rock mass based on damage coefficient. *Rock Mech Rock Eng* 50(3):1–16. <https://doi.org/10.1007/s00603-016-1122-x>
- Nie ZB, Chen JP, Zhang W, Tan C, Ma ZF, Wang FY, Zhang Y, Que JS (2019) A new method for three-dimensional fracture network modelling for trace data collected in a large sampling window. *Rock Mech Rock Eng* 53(3):1145–1161. <https://doi.org/10.1007/s00603-019-01969-4>
- Piggott AR, Elsworth D (1989) Physical and numerical studies of a fracture system model. *Water Resour Res* 25(3):457–462. <https://doi.org/10.1029/WR025i003p00457>
- Pinto A, Da CH (1993) Scale effects in rock mechanics. A. A. Balkema Publishers, Rotterdam
- Shanley RJ, Mahtab MA (1976) Delineation and analysis of clusters in orientation data. *Math Geol* 8(1):9–23. <https://doi.org/10.1007/BF01039681>
- Song SY, Sun FY, Chen JP, Zhang W, Han XD, Zhang XD (2017) Determination of RVE size based on the 3D fracture persistence. *Q J Eng Geol Hydroge* 50(1):60–68. <https://doi.org/10.1144/qjgeh.2016.127>
- Terzaghi RD (1965) Sources of error in joint surveys. *Geotechnique* 15(3):287–304. <https://doi.org/10.1680/geot.1965.15.3.287>
- Wu Q, Kulatilake PHSW (2012) REV and its properties on fracture system and mechanical properties, and an orthotropic constitutive model for a jointed rock mass in a dam site in China. *Comput Geotech* 43:124–142. <https://doi.org/10.1016/j.compgeo.2012.02.010>
- Wu FQ, Deng Y, Wu J, Li B, Sha P, Guan SG, Zhang K, He KQ, Liu HD, Qiu SH (2020) Stress-strain relationship in elastic stage of fractured rock mass. *Eng Geol* 268:105498. <https://doi.org/10.1016/j.enggeo.2020.105498>
- Xu L, Ren Q W (2015) Shear failure mechanism of infilling rock joints and its PFC simulation. *Appl Mech Mater* 723:317–321. <https://doi.org/10.4028/www.scientific.net/AMM.723.317>
- Xu L, Ren QW (2015) Particle flow simulation of direct shear test of rock discontinuities. *Adv Mat Res* 1065–1069:159–163. [https://doi.org/10.4028/www.scientific.net/AMR.1065-1069\(159-163\)](https://doi.org/10.4028/www.scientific.net/AMR.1065-1069(159-163))
- Yang BD, Jiao Y, Lei ST (2006) A study on the effects of microparameters on macroproperties for specimens created by bonded particles. *Eng Computation* 23(6):607–631. <https://doi.org/10.1108/02644400610680333>
- Yang SQ, Huang YH, Jing HW, Liu XR (2014) Discrete element modeling on fracture coalescence behavior of red sandstone containing two unparallel fissures under uniaxial compression. *Eng Geol* 178:28–48. <https://doi.org/10.1016/j.enggeo.2014.06.005>
- Yao W, Cai YY, Yu J, Zhou JF, Liu SY, Tu BX (2019) Experimental and numerical study on mechanical and cracking behaviors of flawed granite under triaxial compression. *Measurement* 145:573–582. <https://doi.org/10.1016/j.measurement.2019.03.035>
- Yong R, Ye J, Li B, Du SG (2018) Determining the maximum sampling interval in rock joint roughness measurements using Fourier series. *Int J Rock Mech Min Sci* 101:78–88. <https://doi.org/10.1016/j.ijrmmms.2017.11.008>
- Yoon J (2007) Application of experimental design and optimization to PFC model calibration in uniaxial compression simulation. *Int J Rock Mech Min Sci* 44(6):871–889. <https://doi.org/10.1016/j.ijrmmms.2007.01.004>
- Zhang LY, Einstein HH (2000) Estimating the intensity of rock discontinuities. *Int J Rock Mech Min Sci* 37(5):819–837. [https://doi.org/10.1016/S1365-1609\(00\)00022-8](https://doi.org/10.1016/S1365-1609(00)00022-8)
- Zhang W, Chen JP, Liu C, Huang R, Li M, Zhang Y (2012) Determination of geometrical and structural representative volume elements at the Baihetan dam site. *Rock Mech Rock Eng* 45(3):409–419. <https://doi.org/10.1007/s00603-011-0191-0>
- Zhang W, Chen JP, Cao ZX, Wang RY (2013a) Size effect of RQD and generalized representative volume elements: a case study on an underground excavation in Baihetan dam, Southwest China. *Tunn Undergr Sp Tech* 35:89–98. <https://doi.org/10.1016/j.tust.2012.12.007>
- Zhang W, Chen JP, Chen HE, Xu DZ, Li Y (2013b) Determination of RVE with consideration of the spatial effect. *Int J Rock Mech Min Sci* 61(7):154–160. <https://doi.org/10.1016/j.ijrmmms.2013.02.013>

- Zhang XP, Jiang YJ, Wang G, Wu XZ, Zhang YZ (2016) Numerical experiments on rate-dependent behaviors of granite based on particle discrete element model. *Rock Soil Mech* 37(9):2679–2686. <https://doi.org/10.16285/j.rsm.2016.09.033>
- Zhang W, Zhao QH, Huang RQ, Ma DH, Chen JP, Xu PH, Que JS (2017a) Determination of representative volume element considering the probability that a sample can represent the investigated rock mass at Baihetan dam site. *China Rock Mech Rock Eng* 50(10):2817–2825. <https://doi.org/10.1007/s00603-017-1248-5>
- Zhang YZ, Wang G, Jiang YJ, Wang SG, Zhao HH, Jing WJ (2017b) Acoustic emission characteristics and failure mechanism of fractured rock under different loading rates. *Shock Vib* 2017:1–13. <https://doi.org/10.1155/2017/5387459>
- Zhang W, Fu R, Tan C, Ma ZF, Zhang Y, Song SY, Xu PH, Wang SN, Zhao YP (2020a) Two-dimensional discrepancies in fracture geometric factors and connectivity between field-collected and stochastically modeled DFNs: A case study of sluice foundation rock mass in Datengxia. *China Rock Mech Rock Eng* 53(5):2399–2417. <https://doi.org/10.1007/s00603-019-02029-7>
- Zhang W, Lan ZG, Ma ZF, Tan C, Que JS, Wang FY, Cao C (2020b) Determination of statistical discontinuity persistence for a rock mass characterized by non-persistent fractures. *Int J Rock Mech Min Sci* 126:104177. <https://doi.org/10.1016/j.ijrmms.2019.104177>
- Zhou Y, Wu SC, Jiao JJ, Zhang XP (2011) Research on mesomechanical parameters of rock and soil mass based on BP neural network. *Rock Soil Mech* 32(12):3821–3826. <https://doi.org/10.1097/RLU.0b013e3181f49ac7>

Publisher's Note Springer Nature remains neutral with regard to jurisdictional claims in published maps and institutional affiliations.